ISSN 1990-7931, Russian Journal of Physical Chemistry B, 2018, Vol. 12, No. 3, pp. 403–411. © Pleiades Publishing, Ltd., 2018.
Original Russian Text © A.E. Galashev, O.R. Rakhmanova, L.A. Elshina, 2018, published in Khimicheskaya Fizika, 2018, Vol. 37, No. 6, pp. 18–27.

STRUCTURE OF CHEMICAL COMPOUNDS. SPECTROSCOPY

Molecular Dynamics Study of the Formation of Solid Al–C Nanocomposites

A. E. Galashev[a], *, O. R. Rakhmanova[a], and L. A. Elshina[a]

[a] *Institute of High-Temperature Electrochemistry, Ural Branch, Russian Academy of Sciences, Yekaterinburg, 620990 Russia*

**e-mail: alexander-galashev@yandex.ru*

Received July 7, 2017

Abstract—Migration of graphene fragments along the aluminum matrix in the solid phase was studied by molecular dynamics. The structure of the Al–C nanocomposite grain was studied by statistical geometry. The distributions of the topological and metric characteristics of truncated polyhedra were calculated for the Al subsystem; the distributions for the polyhedra constructed at the centers of mass of the hypothetical geometrical neighbors were calculated for the carbon subsystem. The graphene fragments are concentrated at the structural grain boundaries. The nanocomposite grains are preferably separated by single-layer graphene rather than by the two-layer graphene membrane.

Keywords: aluminum, graphene, diffusion coefficient, Voronoi polyhedra, molecular dynamics, nanocomposite

DOI: 10.1134/S1990793118030247

INTRODUCTION

Graphene is a material consisting of one atomic layer. It has excellent mechanical properties and can be used to increase the strength of composite materials. Due to its two-dimensional geometry and high strength, as follows from a Young's modulus of 1 TPa, it can effectively restrain the motion of dislocations, increasing the mechanical strength of metals. The conventional methods for the production of cast composite alloys strengthened by disperse particles are complicated by the low wettability of the strengthening particles, their lumping, and nonuniform distribution in the melt. The problem of wettability of carbon particles by molten aluminum can easily be solved by using alkali and alkaline earth metals as reaction media for the synthesis of molten halides (chlorides and fluorides) [1]. The diffusion coefficients of ions in molten halides and aluminum are comparable, which makes it possible to perform the reactions of carbon-containing additives and aluminum at relatively low temperatures (973–1073 K) [2].

In the temperature range 973–1073 K, the chemical reactions of molten aluminum with metal and nonmetal carbides and solid organic substances are feasible. The main products of interaction—alumina and carbon—form under the layer of molten alkali metal chlorides. Alumina forms as a nanopowder in the molten electrolyte (outside the Al matrix), and carbon enters the aluminum melt in large quantities and forms nanosized thin graphene layers that can well be observed on the surface of the molten electrolyte. Note that in the method for the synthesis of the Al–C composite proposed in [1, 2], the Al_2O_3 nanofilms do not form on the Al surface. The presence of these nanofilms significantly affects the contact electrical and thermal resistance [3].

Aluminum and carbon do not interact until the temperature has reached 1373 K. Carbon can be incorporated in aluminum in amounts exceeding the solubility level (0.03 at %) only due to processes at the atomic level. Carbon atoms appear on the aluminum surface and diffuse into aluminum. As the temperature of the real experiment is much lower than the formation temperature of aluminum carbide, the latter cannot form. Inside the aluminum matrix, the components of the molten halide mixture react with molten aluminum in a one-stage process. Carbon that was not incorporated and involved in the interstitial solution forms numerous graphene layers well wetted with liquid Al. Subsequent cooling leads to solidification and formation of the Al–C nanocomposite. The final formation of the nanocomposite can occur in the solid phase. The mechanism of this process is still unknown.

The composition and structure of metal–graphene composite materials were studied by scanning electron microscopy on modern microscopes, by Raman spectroscopy, on an optical profilometer profilograph, and by reflection electron diffraction [1, 2]. The introduction of 1 to 2 wt % graphene in aluminum increases the strength, hardness, and elasticity of aluminum–graphene composites twofold. Further increase to 5 wt % graphene in the metal matrix leads to an increase in

the electrochemical activity, which makes it possible to use metal–graphene electrodes in new generation electrochemical devices [4, 5].

Recently, a nanolayer composite composed of alternating layers of metal (copper or nickel) and monolayer graphene was created [6]. A single-layer sheet of graphene was grown on a metal substrate by chemical vapor deposition (CVD). One metal layer was attached to this structure. This procedure was repeated several times and resulted in multilayer metal–graphene. This material shows ultrahigh tensile strength, which reaches 1.5 GPa for the copper–graphene nanocomposite and 4.0 GPa for the nickel–graphene material. This is higher than the strength of pure copper and annealed nickel by a factor of 5.3 and 8.2, respectively. The ultrahigh strength of these metal–graphene nanolayer structures shows the efficiency of graphene in blocking the motion of dislocations across the metal–graphene interface.

The goal of this study was to investigate the grain formation of the Al–C nanocomposite in the solid phase and explain the most important properties of the obtained material based on the data on the detailed structure of the grain under study.

COMPUTER MODEL

The formation of the structural grain of the Al–C nanocomposite was simulated by the classic molecular dynamics method. The interatomic interactions in graphene were represented by the second-generation Brenner many-body potential [7]. The energy of the pair interaction of the i and j atoms including the effects of other atoms (many-body effects) is recorded as

$$V_{ij} = f_{ij}^{C}(r_{ij})\left(f_{ij}^{R} - \bar{b}_{ij} f_{ij}^{A}\right), \tag{1}$$

$$\begin{aligned} f_{ij}^{R} &= \left(1 + Q/r_{ij}\right) A \exp\left(-\alpha r_{ij}\right), \\ f_{ij}^{A} &= \sum_{n=1}^{3} B_n \exp\left(-\lambda_n r_{ij}\right), \end{aligned} \tag{2}$$

where r_{ij} is the distance between the i and j atoms, A and B are the energy characteristics of repulsion and attraction, and $\bar{b}_{ij}$ is the bond order parameter that takes into account the many-body interactions. The $\bar{b}_{ij}$ parameter is specified as

$$\begin{aligned} \bar{b}_{ij} &= \frac{1}{2}\left(b_{ij}^{\sigma-\pi} + b_{ji}^{\sigma-\pi}\right) + \Pi_{ij}^{RC} + b_{ij}^{DH}, \\ b_{ij}^{\sigma-\pi} &= \left(1 + \sum_{k\neq i,j} f_{ik}^{C} g_{ijk}\right)^{-1/2}, \\ g_{ijk} &= \sum_{i=0}^{5} \beta_i \cos^{i}(\theta_{ijk}). \end{aligned} \tag{3}$$

The $b_{ij}^{\sigma-\pi}$ parameter depends on the local coordination of atoms around the i atom and the θ_{ijk} angle between the i, j, and k atoms. This function of the π bond is symmetric for graphene, graphite, and diamond, $b_{ij}^{\sigma-\pi} = b_{ji}^{\sigma-\pi}$. The β_i coefficients in the spline function g_{ijk}, which characterizes the bending of the bonds, were fitted to the experimental data for graphite and diamond. The additional contributions to energy created by defects, for example, vacancies, are calculated in terms of the Π_{ij}^{RC} parameter. It is generally taken that $\Pi_{ij}^{RC} = 0$. The dihedral bending function b_{ij}^{DH} depends on the local conjugation. It is zero for diamond, but plays an important role in graphene description. This function is recorded as

$$b_{ij}^{DH} = \frac{T_0}{2} \sum_{k,l\neq i,j} f_{ik}^{C} f_{jl}^{C} \left[1 - \cos^2(\vartheta_{ijkl})\right], \tag{4}$$

where T_0 is a parameter, f_{ij}^{C} is the truncation function, and ϑ_{ijkl} is the dihedral angle formed by four atoms denoted by the indices i, j, k, and l:

$$\cos(\vartheta_{ijkl}) = \boldsymbol{\eta}_{jik} \boldsymbol{\eta}_{ijl}, \tag{5}$$

$$\boldsymbol{\eta}_{jik} = \frac{\left[\mathbf{r}_{ji}\mathbf{r}_{ik}\right]}{\left|\mathbf{r}_{ji}\right|\left|\mathbf{r}_{ik}\right|\sin(\theta_{ijk})}; \tag{6}$$

here $\boldsymbol{\eta}_{jik}$ and $\boldsymbol{\eta}_{ijl}$ are the unit vectors perpendicular to the triangles formed from the atoms with the corresponding indices, $\mathbf{r}_{ij}$ is the vector drawn from the nucleus of the i atom to the nucleus of the j atom, and θ_{ijk} is the angle between the i, j, and k atoms. In planar graphene, the dihedral angle ϑ_{ijkl} equals either 0 or π, and hence $b_{ij}^{DH} = 0$. The bending of the graphene layer gives a contribution defined by b_{ij}^{DH}. The values of all parameters of (1)–(6) were given in [8]. The first-generation Brenner potential [7] is restrictive at decreased interatomic distances and limits the possibility of modeling the processes involving energetic atomic collisions. The potential was corrected, which made it possible to correctly describe hydrocarbonates and model the reactions along with the reproduction of equilibrium or quasiequilibrium states of pure carbon. In the modified version, the potential explicitly includes the term containing a dihedral angle, which describes an important interaction of the π orbitals. This considerably improved the description of the moduli that characterize the bending of graphene, but regretfully did not correct Young's moduli [8]. The molecular dynamics (MD) simulation of graphite and graphene was considered in [9–13].

The interactions between the Al atoms in the model are described using the Finnis–Sinclair potential [14]. This potential is justified from the viewpoint of the electron theory of solids. The potential energy of an atomic system U is represented as the sum of the contributions of the pair interactions of atoms U_p and the

many-particle contribution U_N identified with the energy of conduction electrons:

$$U = U_p + U_N = \frac{1}{2}\sum_{i}^{N}\sum_{j,i\neq j}^{N}\left[\left(r_{ij}-c\right)^2\left(c_0 + c_1 r_{ij} + c_2 r_{ij}^2\right)\right] - A\sum_{i}^{N}\left\{\sum_{j,i\neq j}\left(r_{ij}-d\right)^2\right\}^{1/2}, \quad (7)$$

where N is the number of atoms; r_{ij} is the distance between the i and j atoms; c, c_0, c_1, c_2, d, and A are the parameters of the potential [15]; and c and d are the truncation radii for U_p and U_N.

The interaction between the Al and C atoms was specified in terms of the Lennard-Jones potential, whose parameters were taken from [16].

The behavior of the graphene fragments in the structural grain of aluminum is considered here in the model with periodic boundary conditions. In this case, these conditions were used to model a grain (basic cell) (but not a homogeneous conventionally infinite system) separated from other grains by the boundaries formed by close-packed planes or their edges. The calculations were performed for a system of 1296 Al and 114 C atoms. The concentration of the C atoms for this system was 3.77 wt %; i.e., it was approximately identical to the analogous characteristic of the experimental nanocomposite samples. The initial configuration of the system was formed from 13 close-packed (111) planes of aluminum. The graphene fragments containing 19 C atoms were embedded in six nonadjacent planes. The graphene fragment was formed from five hexagonal honeycomb cells. Each graphene fragment was located in the middle part of the (111) plane of aluminum. The distances between the Al and C atoms in this plane were not shorter than the equilibrium distance $r^0_{\mathrm{Al-C}} = 2.97$ Å of the corresponding Morse potential [17]. This distance does not exceed the distance between the close-packed planes in aluminum ($r_{\mathrm{Al-Al}} = 3.2$ Å). The external surface of the nanocomposite initially did not contain any C atoms; i.e., it was formed by the perfect (111) Al planes. The calculations were performed in the *NVT* ensemble at $T = 300$ K at a time step of $\Delta t = 10^{-16}$ s.

The structures obtained as a result of structure relaxation were analyzed by the statistic geometry method. Given the size of the system and duration of MD calculation, the Voronoi polyhedra (VPs) were constructed every 10^4 time steps for 500 Al atoms closest to the center of mass of the simulated structural grain. The polyhedra were built within the final 2.5 million time steps; the total number of VPs was 125000. For the C atoms in this system, the VPs cannot be built by the conventional technique because of the small number of atoms in the carbon subsystem and the specific arrangement of C atoms over the sites of the honeycomb cells and the arrangement of graphene fragments in the MD cell. A typical case of obstacles to construction of VPs here is the absence of geometrical neighbors in one of the half-spaces allocated for constructing the VPs. Therefore, in constructing the VPs for C atoms, we used the method proposed in [18, 19]. In this method, the VP is constructed based on the coordinates of the center of mass of the candidate atoms for the role of geometrical neighbors, but not by the coordinates of the center of one of the atoms (the central atom).

The calculations were performed using the codes of the LAMMPS software package [20]. The calculations were performed on a URAN hybrid cluster-type computer at the Krasovskii Institute of Mathematics and Mechanics, Ural Branch, Russian Academy of Sciences, with a peak performance of 216 Tflop/s and 1864 CPUs.

RESULTS OF CALCULATION

In the scanning electron microscopy (SEM) method, a thin electron beam (probe) is directed to the sample to be analyzed, generating low-energy secondary electrons collected by a detector. The intensity of the electrical signal of the detector mostly depends on the topography of the sample in the interaction region. As a result, a map of the relief of the zone being analyzed is obtained. Figure 1 shows the presence of graphene films in the surface region of the aluminum–graphene composite detected by SEM. It can be seen that the graphene sheets do not lie in the same plane; they can form piles (Fig. 1a), can be bent and connected with one another (Fig. 1b).

In view of the nonequilibrium initial state of the system, we determined the self-diffusion coefficient D for Al and C atoms in the final quarter of MD calculation, whose duration was 0.25 ns. The D value was calculated from the change in the mean square atomic displacement with time. The obtained self-diffusion coefficients ($D_{\mathrm{Al}} = 10.32 \times 10^{-10}$ m^2/s, $D_{\mathrm{C}} = 5.84 \times 10^{-10}$ m^2/s) indicate that the mobility of the metal atoms significantly (by a factor of 1.76) exceeds the mobility of carbon inclusions with time.

By the end of the calculation with a duration of 10^6 time steps, the structural grain of the Al–C nanocomposite acquired an oval shape (Fig. 2). The transformation of the cube into an ellipsoid is caused by the structural relaxation, which leads to a decrease in the energy of the system due to the change in the external shape of the grain. During the structural relaxation, all graphene fragments moved either to the surface of the grain or to a region close to its boundary. The right part of Fig. 2 shows the arrangement of the carbon component in the system after the removal of Al atoms. It can be seen that the graphene fragments can be connected with one another, forming a curved part of the surface (right top and bottom, Fig. 2). In addi-

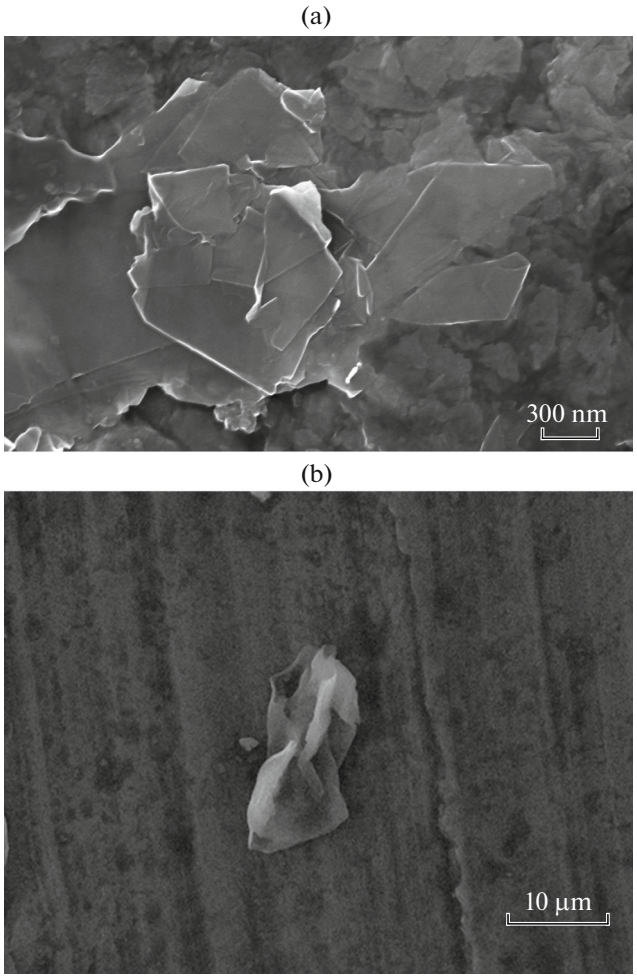

Fig. 1. SEM image of graphene films on the surface of the aluminum–graphene composite after rolling (high magnification).

tion, the graphene fragments near the grain surface can be covered with one layer of Al atoms. This arrangement of graphene in the structural grain is also characteristic of the real Al–C nanocomposite, as shown by the optical image of its cross-section.

The distribution of VPs according to the number of faces (n distribution) shows the most probable number of nearest geometrical neighbors in the system, which is $n_{mp} = 15$ for the Al subsystem (Fig. 3). There are polyhedra containing from 9 to 23 faces in this rather wide spectrum. The average number of faces in the VP corresponds to $\overline{n} = 14.77$. The fraction of 16-hedra (17.6%) is almost equal to that of 15-hedra (18.9%). A completely different type of n distribution was obtained for the carbon subsystem, where the VPs were built around the center of mass of the C atoms supposed to be geometrical neighbors. Here the most probable number of geometrical neighbors is $n_{mp} = 4$ (insert, Fig. 3). However, the percent of heptahedra (16.3%) and pentahedra (14.2%) is also comparable to that of tetrahedra (20.4%). The average number of faces in the VP is $\overline{n} = 7.31$.

The small-scale thermal fluctuations give rise to small geometrical elements (edges and faces) in the VPs [21]. The presence of these elements complicates the structure analysis. Let us consider the statistical analysis data for the structure of the nanocomposite obtained by eliminating small geometrical elements in the polyhedra (truncation of polyhedra). The maximum in the distribution of polyhedra over the number of faces for the aluminum subsystem shifts to the left by $n = 14$ after excluding the edges with the length $l \le 0.5\overline{l}$, where $\overline{l}$ is the average edge length. The use of elimination leads to an asymmetric n distribution. The fraction of polyhedra with $n < 14$ here was 42.7%, and that of polyhedra with $n > 14$ was 38.8%. Moreover, the number of types ($4 \le n \le 13$) of the former exceeded the corresponding number of types ($15 \le n \le 21$) of the latter. After truncation of the VP for the carbon subsystem, an extremely poor n spectrum with $n < 10$ was obtained, in which the majority of polyhedra each contained four or five faces. The average number of faces in the truncated polyhedra (TPs) was $\overline{n} = 12.96$ for the Al subsystem and $\overline{n} = 4.89$ for the C subsystem. The faces of these TPs are mainly formed using the direct neighbors, i.e., the neighbors for which the line through the centers of two atoms (one of which is central) intersects the face of the polyhedron of the nearest neighbor. The predominance of the polyhedra formed by a small number of direct neighbors in the n spectrum indicates that the C atoms concentrate in a limited number of regions of the system.

As for the distribution of faces according to the number of sides (m distribution), the hexagons (31.1%) slightly dominate over the pentagons (30.9%) in the Al subsystem (Fig. 4). Here, the number of neighbors around the rotational symmetry axes of the polyhedra (the number of sides m in the faces) varies from 3 to 10. The average number of sides in the faces is $\overline{m} = 5.53$. For the C subsystem (insert, Fig. 4), the three-sided faces dominate (46.1%) in the m distribution; then follow the quadrangles (19.5%). The calculated m spectrum terminates at $m = 9$. The average number of sides in the faces of the C subsystem is $\overline{m} = 4.14$. None of the subsystems shows a clearly expressed fivefold symmetry axis; i.e., none of them is a disordered medium.

The maximum of m distribution for truncated polyhedra is at $m = 5$ for the Al subsystem and $m = 4$ for the carbon subsystem. Then follow hexagons, whose number is 6.5% smaller than that of pentagons in the aluminum subsystem, and triangles, whose number is 11.1% smaller than the number of quadrangles in the carbon subsystem. Triangles are often excluded for both subsystems. The proportion of quadrangles is 1.6 times smaller than that of triangles for the Al subsystem and 6.0 times smaller for the C subsystem. The average number of sides in the faces of

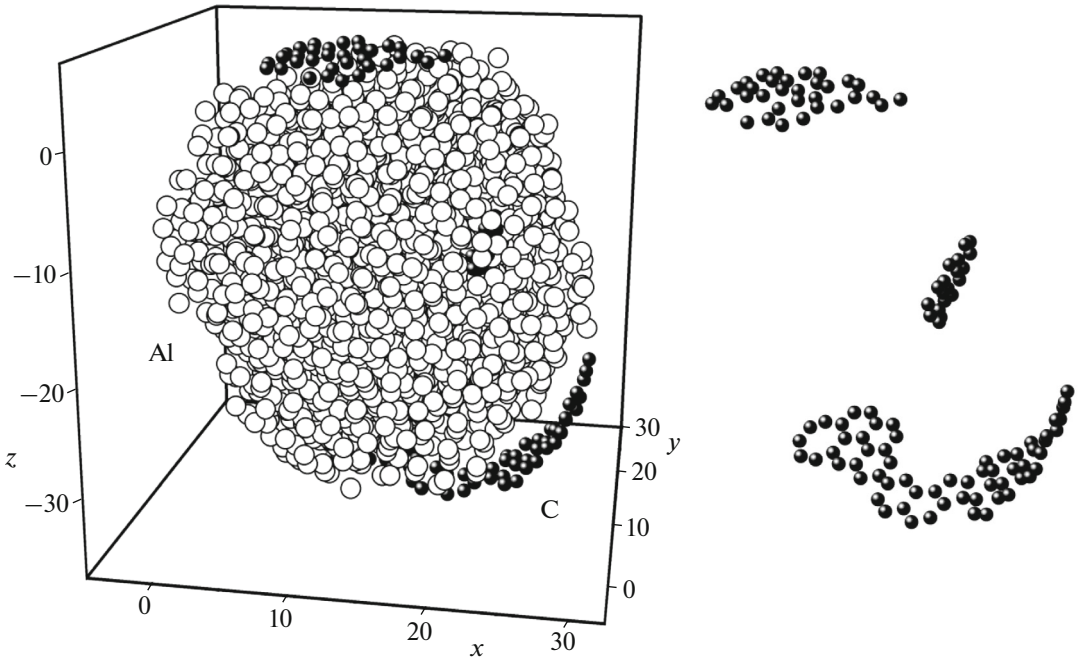

Fig. 2. Configuration of the structural grain of the Al–C nanocomposite referring to the moment of time 1 ns; the structure of the carbon subsystem is shown on the right; the atomic coordinates are presented in angstroms.

truncated polyhedra was $\bar{m} = 5.27$ for the Al subsystem and $\bar{m} = 4.27$ for the C subsystem.

Let us have the detailed structure of the nanocomposite complemented with metric characteristics. The spectra of the surface areas and volumes of polyhedra are well approximated by the Gaussian distributions (dashed lines, Fig. 5). The transition to the theoretical representation of these spectra allows us to move away from a particular system and the number of VPs used to construct the distributions. The most probable surface areas and volumes of VP obtained from the Gaussian distributions are $S_{mp} = 1.16$ nm^2 and $V_{mp} = 0.073$ nm^3.

The angular distribution (θ distribution) was constructed for the nearest geometrical neighbors, which give the faces of the VP. The vertex of the θ angle coincides with the center of the VP. In the angular distribution of the nearest neighbors of the aluminum subsystem, there are four peaks and a shoulder in the vicinity of the angle θ = 150° against the continuous back-

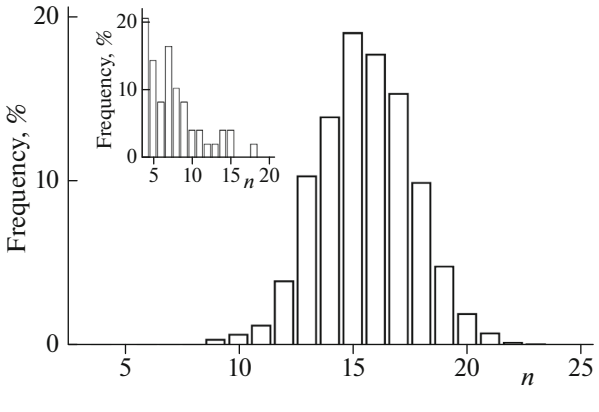

Fig. 3. Distribution of the Voronoi polyhedra according to the number of faces in the aluminum matrix. Insert: distribution of polyhedra according to the number of faces for the carbon subsystem based on the construction of polyhedra for the centers of mass of the hypothetical geometrical neighbors.

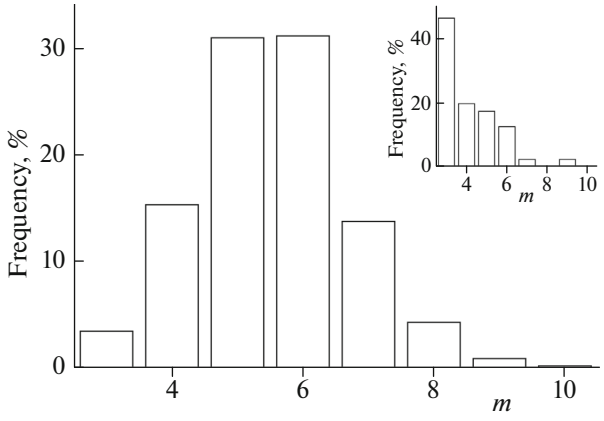

Fig. 4. Distribution of faces of the VP according to the number of edges in the aluminum matrix. Insert: distribution of polyhedron faces according to the number of edges for the carbon subsystem based on the construction of polyhedra for the centers of mass of the hypothetical geometrical neighbors.

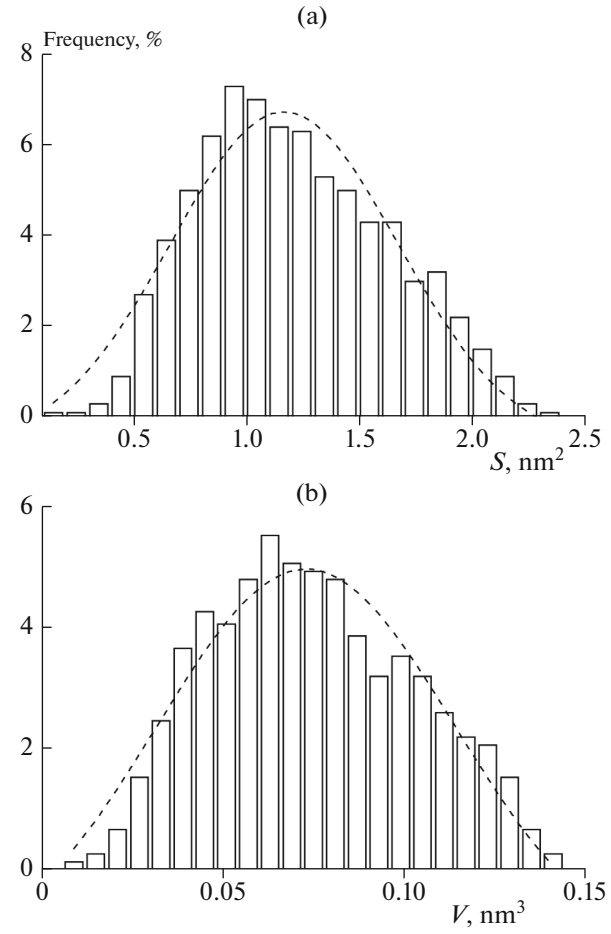

Fig. 5. Distributions of the areas of faces (a) and volumes of Voronoi polyhedra (b) in the aluminum matrix.

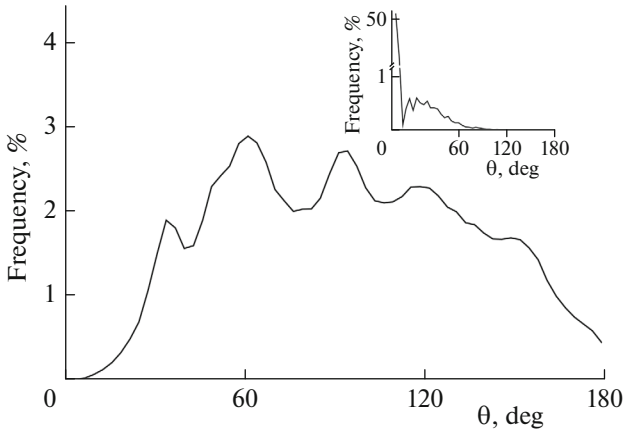

Fig. 6. Angular distribution of the nearest geometrical neighbors in the aluminum matrix. Insert: θ distribution for the carbon subsystem based on the construction of polyhedra for the centers of mass of the hypothetical geometrical neighbors.

ground (Fig. 6). The peaks are generally repeated with a multiplicity of 30°; i.e., they lie at 60°, 90°, and 120°. However, the first peak is slightly shifted to the right and lies at 36°. A basically different type of θ distribution was obtained for the C subsystem (insert, Fig. 6). Here, the linear arrangement of triples of C atoms with $\theta = 0°–3°$ is clearly dominant. These are up to 66.5% of the total number of θ angles. Another 26.6% of all θ angles are in the range 3°–6°. Thus, all other angles account for only 6.9%. The angular distribution in this case extends only to $\theta = 90°$. This indicates that the compact arrangement of the C atoms is mainly trilateral.

The distribution of the distances to the nearest geometrical neighbors (L distribution) in the Al matrix is a continuous spectrum with three peaks at 0.27, 0.47, and 0.92 nm (Fig. 7). The first of these distances is slightly shorter than the distance between the nearest neighbors in polycrystalline Al (0.286 nm). The reduction of the interatomic Al–Al distances in the nanocomposite is explained as follows. As nanomaterials have a high surface area, the formation of phases with a smaller surface energy and hence with denser packing (that is, smaller volume per atom) is preferable. The average distance to the second-order neighbors in the resulting nanocomposite is longer than in the real Al crystal (0.404 nm). This is due to the presence of graphene inclusions in the aluminum matrix. A strong deformation forms clusters in solid Al [22]. The size of these deformation clusters is 0.5–2.5 nm. The long-term structural order is maintained within one cluster; i.e., this distance is limited by the size $R_{cl} = 1.25$ nm. The third peak lies at $r_{m3} < R_{cl}$ in the L distribution and can reflect the long-range ordering in the Al–C nanocomposite.

To trace the formation of the grain boundary, we performed MD simulations of two identical grains (each of 1410 atoms) brought in contact along the boundaries containing graphene fragments. Thus, a region of double graphene layer was formed in the zone of grain contact at the initial moment of time. The initial grain for this calculation was obtained as a result of MD simulation after 1-ns evolution. This computer experiment was supposed to answer the question whether two-layer graphene can form in the grain boundary region. This question arose in connection with the observation of a number of square "points" in the optical image of the transverse section of the aluminum–graphene composite in the region of the graphene film. The observation of the evolution of two contact grains for 0.5 ns does not give a positive answer to this question (Fig. 8). The grain contact area increased due to the sliding of graphene fragments relative to one another and their subsequent connection with formation of a single-layered graphene boundary. The result of this sliding was mutual displacement of grains. This calculation showed that the existence of only single-layered graphene arranged on the grain boundary is preferable in the Al–C nanocomposite. The calculated self-diffusion coefficient of atoms in paired grains is several orders of magnitude lower than in the case of the structural rearrangement of the grain

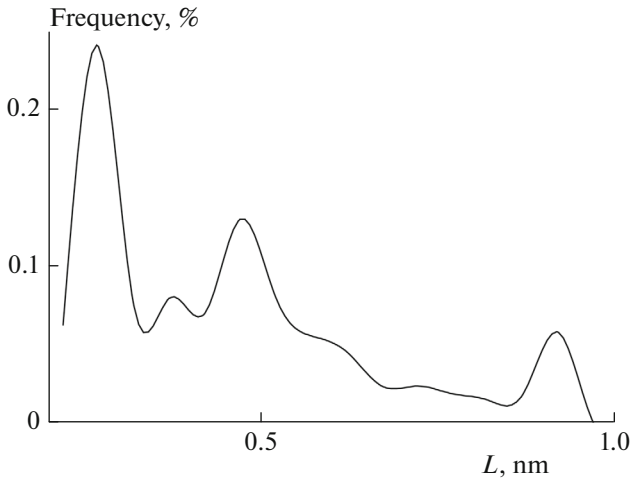

Fig. 7. Distribution of distances to the nearest geometrical neighbors represented by Al atoms in the aluminum matrix.

associated with the motion of graphene fragments. For Al atoms, this value was estimated at 5.4×10^{-13} m^2/s. For C atoms, the D coefficient cannot be estimated because the slope of the approximated part of the $\left\langle (\Delta r)^2 \right\rangle (t)$ function is too small.

DISCUSSION

The macroscopic properties of materials are the main criteria for their application. However, the macroscopic properties of materials are determined by their interactions at small scales of length. To design new composite materials, it is important to understand and evaluate the significance of the relationship between the small-scale effects, leading to various macroscopic effects. The experimental testing is expensive and time-consuming and sometimes simply inaccessible. Therefore, it is promising to use computational methods for modeling and predicting the macroproperties of materials. This study presents the results of investigation of the structure and properties of the new material at the nanosized level.

The model of the Al subsystem used here shows only weak tendency toward a decrease in the interaction with the distance. The long-range interactions between the metal atoms stimulate the movement of graphene sheets along the (111) close-packed planes of the fcc lattice of aluminum. Graphene tends to occupy a more vacant space in the matrix and moves toward the grain boundaries. Its motion along the boundary is due to the sheet curvature. Because of the limited vacant space on the grain boundary, the graphene sheets contact, which eventually leads to their merging.

The experiment showed that the introduction of Al in a thin-film nanocomposite based on diamond-like carbon leads to a sharp decrease in the C–C sp^3 binding and an increase in the C–C sp^2 binding [23]. Thus, there is a general decrease in the sp^3/sp^2 ratio and the hardness of the nanofilm. Aluminum in a doped nanomaterial exists as an element, but not as a compound. In the Al–C nanocomposite under study, the aluminum effect on the carbon material is opposite. In this case, Al does not appear as an alloying element, but as a matrix base; i.e., the system has much more Al than C atoms. The Al atoms are extremely reactive. The edge C atoms of the graphene fragments also tend

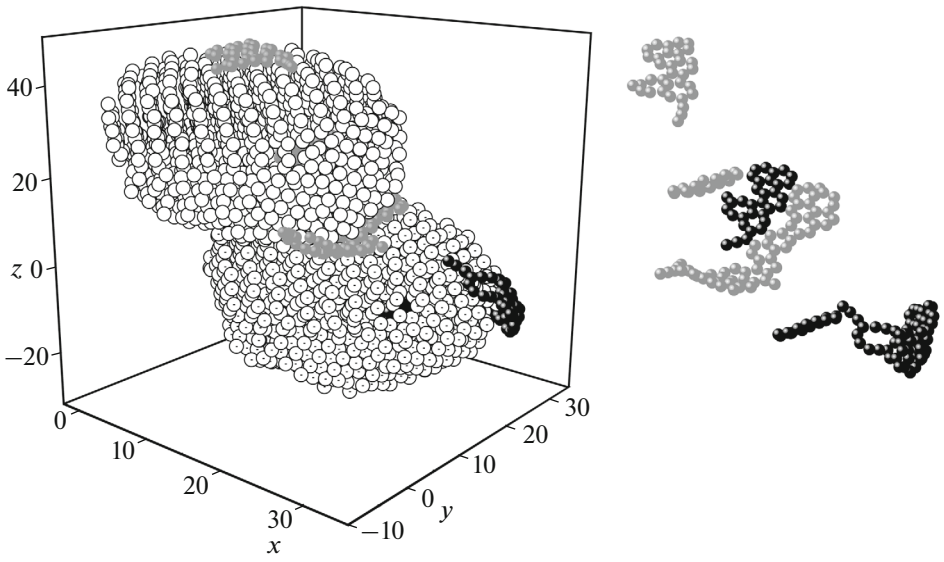

Fig. 8. Configuration of two contacting structural grains of the Al–C nanocomposite obtained at a time 0.5 ns; the structure of the carbon subsystem is shown on the right. The C atoms of the upper grain are shown in gray; the C atoms of the lower grain are shown in black; the atomic coordinates are given in angstroms.

to bonding. As a result, a strong covalent bond can form between them and the nearest Al atoms. The formation of this bond leads to an increase in the strength of the nanomaterial. The Al atoms located above and below the graphene sheets do not form a chemical bond with the carbon atoms; i.e., in these places the metal is elemental Al. This imparts higher plasticity to the nanocomposite relative to pure aluminum. As a result, the presence of graphene fragments in the aluminum matrix leads to an increase in the strength of the formed nanocomposite and simultaneous enhancement of its plasticity.

For structure relaxation due to the motion of graphene fragments along the aluminum matrix and in the case of these fragments sliding along the boundary of two contacting grains, the self-diffusion coefficients for C atoms are substantially lower than for Al atoms. This is due to the long-range interaction in aluminum and formation of a chemical bond corresponding to this interaction. The strong covalent bond, in turn, allows graphene fragments to retain their integrity and to glide between the close-packed planes in a solid. It should be emphasized that it is exactly the specific motion in the aluminum matrix that allows the graphene film to remain in the nanocomposite.

Similar graphene fragments were also created in the (100) planes of the aluminum matrix, with the pure metal plane alternating with the graphene-containing plane. In this case, however, the graphene sheets were always destroyed. The carbon atoms were ultimately uniformly distributed throughout the whole volume of the metal matrix. Thus, the formation of a graphene film on the grain boundary of the Al–C nanocomposite is associated with the motion of graphene fragments along the close-packed planes. However, individual carbon atoms are also present in the nanocomposite.

The exit of graphene fragments to the surface of the structural grain and hence the abundance of graphene on the surface of the Al–C nanocomposite prevents this composite material from being oxidized. As graphene does not interact with oxygen, an oxide film does not form on the surface of the Al–C nanocomposite. The material obtained by the authors of [1, 2] has a characteristic metallic luster. It was not oxidized in air for 1.5 years. In addition, the presence of such a strong material as graphene on the grain boundaries substantially increases (up to twofold) the strength and hardness of the new material compared to those of pure aluminum. At the same time, the elasticity of the material increases, suggesting the possibility of obtaining nanowires, which cannot be manufactured from polycrystalline aluminum because of its high brittleness.

We showed that graphene fragments in the grain have different shapes, sizes, and orientations. Due to the fairly chaotic mutual orientation of the planes of graphene fragments, they are dislocated with difficulty when the structural grain melts. The inertness of graphene inclusions during the melting of the aluminum matrix is also the consequence of the thermal stability of graphene, whose melting point is 4900 K [24]. Due to this inertness of graphene inclusions, the material retains its unusual properties after the melting. Indeed, the new Al–C material can be obtained with a large size by melting while preserving the original properties. If the graphene film is present on the boundary of each contacting grain, the sliding between them leads to a displacement and cross-linking of graphene fragments, as a result of which the grain boundary is separated by single-layer graphene.

CONCLUSIONS

The Al–C nanocomposite was synthesized due to the creation of fundamentally new external conditions of interaction for Al and C atoms. This situation is quite similar to that in the earth's crust and leads to significant differences between chemistry and geochemistry. A definite part of the earth's crust contains the chemical elements not only in the form of salts (minerals) or solutions, but also in quite diverse forms—systems with relatively stable chemical equilibria. The elements in these systems can form compounds that exhibit the properties that are unusual for traditional perception. Moreover, these properties are preserved even after the forms of coexisting elements are destroyed. The simple use of all chemical regularities for the behavior of chemical elements in the Earth does not lead to adequate conclusions.

The present study showed that the graphene layers that formed in the Al melt under certain conditions and are uniformly distributed over the aluminum matrix are capable of moving. The graphene fragments move along the (111) planes of the Al structural grain to its boundary without losing the C atoms and join the same fragments, while being deformed and fixed on the grain boundary. The detailed structure of the formed nanocomposite was investigated.

Thus, the present paper showed that the final stage of structural relaxation can occur in the solid phase, which involves the drift of graphene fragments in the Al matrix when a new Al–C composite material forms. Under the conditions that favor the mutual sliding of grains, graphene that separates them becomes single layer in the Al–C nanocomposite. The origin of the unusual physicochemical properties of the structural grain of the nanocomposite was explained based on its structure.

ACKNOWLEDGMENTS

The experimental part of this work was performed using the equipment of the Shared Access Center "Composition of Compounds" (based on the Solid Oxide Fuel Cells Laboratory, Institute of High-Temperature Electrochemistry, Ural Branch, Russian Academy of Sciences).

REFERENCES

1. L. A. Yolshina, R. V. Muradymov, I. V. Korsun, G. A. Yakovlev, and S. V. Smirnov, J. Alloys Compd. **663**, 449 (2016).
2. L. A. Yolshina, R. V. Muradymov, E. G. Vovkotrub, and S. V. Smirnov, Diamond Rel. Mater. **5**, 1 (2015).
3. A. G. Vikulov, D. G. Vikulov, S. Yu. Mesnyankin, and A. Yu. Fel'dman, High Temp. **53**, 36 (2015).
4. A. V. Eletskii, V. Yu. Zitserman, and G. A. Kobzev, High Temp. **53**, 130 (2015).
5. A. E. Galashev and O. R. Rakhmanova, High Temp. **54**, 11 (2016).
6. Y. Kim, J. Lee, M.-S. Yeom, J.-W. Shin, H. Kim, Y. Cui, J. W. Kysar, J. Hone, Y. Jung, S. Jeon, and S.-M. Han, Nat. Commun. **4**, 2114 (2013).
7. D. W. Brenner, Phys. Rev. B **42**, 9458 (1990).
8. D. W. Brenner, O. A. Shenderova, J. A. Harrison, S. J. Stuart, B. Ni, and S. B. Sinnott, J. Phys: Condens. Matter **14**, 783 (2002).
9. N. D. Orekhov and V. V. Stegailov, High Temp. **52**, 198 (2014).
10. E. Burgos, E. Halac, and H. Bonadeo, Chem. Phys. Lett. **298**, 273 (1998).
11. S. J. Stuart, A. V. Tutein, and J. A. Harrison, J. Chem. Phys. **112**, 6472 (2000).
12. A. E. Galashev and V. A. Polukhin, Phys. Solid State **55**, 1733 (2013).
13. A. E. Galashev and S. Yu. Dubovik, Phys. Solid State **55**, 1976 (2013).
14. M. W. Finnis and J. E. Sinclair, Philos. Mag. A **50**, 45 (1984).
15. C.-F. Zhu, X.-R. Zhang, Y.-H. Wei, P. Yu, X.-J. Zhang, J.-L. Zhang, J. Aeronaut. Mater **23** (2), 25 (2003).
16. S. Xiao and W. Hou, Phys. Rev. B **73**, 115406 (2006).
17. T.-H. Fang and J.-H. Wu, Comput. Mater. Sci. **43**, 785 (2008).
18. A. N. Novruzov, O. R. Rakhmanova, O. A. Novruzova, and A. E. Galashev, Russ. J. Phys. Chem. B **2**, 115 (2008).
19. A. Y. Galashev, Mol. Simul. **36**, 273 (2010).
20. S. Plimpton, J. Comput. Phys. **117**, 1 (1995).
21. V. P. Skripov and A. E. Galashev, Russ. Chem. Rev. **52**, 97 (1983).
22. Z. A. Samoilenko, N. N. Ivakhnenko, E. I. Pushenko, E. G. Pashinskaya, and V. N. Varyukhin, Phys. Solid State **58**, 223 (2016).
23. S. Zhang, Y. Q. Fu, X. L. Bui, and H. J. Du, Int. J. Nanosci. **3**, 797 (2004).
24. A. E. Galashev and O. R. Rakhmanova, Phys. Usp. **57**, 970 (2014).

Translated by L. Smolina